mathematics

Article

Fixed-Time Controller for Altitude/Yaw Control of Mini-Drones: Real-Time Implementation with Uncertainties

Moussa Labbadi [1,*], Chakib Chatri [1], Sahbi Boubaker [2] and Souad Kamel [2]

[1] Univ. Grenoble Alpes, CNRS, Grenoble INP, GIPSA-Lab, 38000 Grenoble, France
[2] Department of Computer & Network Engineering, College of Computer Science and Engineering, University of Jeddah, Jeddah 21959, Saudi Arabia; sboubaker@uj.edu.sa (S.B.)
* Correspondence: moussa.labbadi@grenoble-inp.fr

Abstract: Gradually, it has become easier to use aerial transportation systems in practical applications. However, due to the fixed-length wire, recent studies on load-suspended transportation systems have revealed some practical constraints, especially when using quadrotor unmanned aerial vehicles (UAVs). By actively adjusting the distance between the quadrotor and the payload, it becomes possible to carry out a variety of challenging tasks, including traversing confined spaces, collecting samples from offshore locations, and even landing a payload on a movable platform. Thus, mass variable aerial transportation systems should be equipped with trajectory tracking control mechanisms to accomplish these tasks. Due to the above-mentioned reasons, the present paper addresses the problem of the altitude/yaw tracking control of a mini-quadrotor subject to mass uncertainties. The main objective of this paper is to design a fixed-time stable controller for the perturbed altitude/yaw motions, based on recent results using the fixed-time stability approach. For comparison reasons, other quadrotor motion controllers such as dual proportional integral derivative (PID) loops were considered. To show its effectiveness, the proposed fixed-time controller was validated on a real mini-quadrotor under different scenarios and has shown good performance in terms of stability and trajectory tracking.

Keywords: fixed-time stability; altitude/yaw tracking control; mini-drone; uncertainties

MSC: 93-11

Citation: Labbadi, M.; Chatri, C; Boubaker, S.; Kamel, S. Fixed-Time Controller for Altitude/Yaw Control of Mini-Drones: Real-Time Implementation with Uncertainties. *Mathematics* **2023**, *11*, 2703. https://doi.org/10.3390/math11122703

Academic Editor: António Lopes

Received: 14 April 2023
Revised: 23 May 2023
Accepted: 9 June 2023
Published: 14 June 2023

1. Introduction

Drones, also known as unmanned aerial vehicles (UAVs), have garnered significant attention in recent years due to their ability to be used in various domains including agriculture, sports, spatial imagery, highway monitoring, congestion management in smart cities, and indoor (goods inventory) and outdoor (last-mile delivery) logistics [1,2].

Issues: The proliferation of drones has also resulted in a myriad of security and privacy concerns [3,4]. One of the primary security issues is related to the devices integrated into drones, such as sensors, Bluetooth, and RFID tags, which are vital components of drones that aid in data collection and ensure a safe flight. However, these sensors can be exploited by cyber-attackers to gain unauthorized access and/or disrupt the functioning of the drone. Communication links, such as UAV networks, GPS, and satellites, also pose significant security risks. Often operating over insecure Wi-Fi networks, drones become easy targets for cyber-attacks. Another potential security loophole is the use of RFID technology. Often integrated into drone chips without standard security controls, these devices can be modified, read, or manipulated by hackers, posing serious security threats. Alongside these security issues, privacy concerns are also prevalent. Drones are capable of capturing high-resolution images and videos, which could lead to unwarranted surveillance and privacy leaks if not managed appropriately.

Countermeasures: Given the multifaceted security and privacy issues associated with drones, a range of countermeasures have been proposed and are being actively developed [3,4]. Various detection mechanisms and threat estimate models have been designed to identify cyber-attacks promptly and accurately. When coupled with intrusion detection systems, these systems offer comprehensive solutions to safeguard drones from active security threats such as DoS/DDoS attacks, jamming attacks, and more. Specific countermeasures also target individual types of attacks. For example, RAIM, a game-theoretic countermeasure, and various cryptographic solutions have been proposed to combat GPS jamming and spoofing. Similarly, enhancing existing sensor management systems and securing UAV ground and terrestrial communication are among the many strategies employed to address sensor security issues and Wi-Fi security concerns. Measures to protect RFID threats include RFID threat countermeasure frameworks involving cryptographic algorithms and non-cryptographic schemes. In the face of privacy leaks via photos, various detection techniques such as drone tracking, speech extraction, and sound detection have been proposed.

Limitations: Despite the numerous countermeasures developed to address drone security and privacy issues, several limitations persist in the current solutions. The current detection and defense mechanisms, though sophisticated, may still not be swift and effective enough to promptly detect and neutralize novel, sophisticated threats. The security challenges associated with communication links and drone components, particularly concerning RFID technology integration, require more advanced, comprehensive, and integrated solutions than are currently available. In addition, the measures designed to mitigate the privacy risks associated with drone photography need to be more robust and capable of effectively preventing unwarranted surveillance and the collection of sensitive information.

Robust flight control systems are needed to monitor UAVs' trajectories in the presence of various disturbances such as wind. The aim of these control systems is to achieve a certain level of autonomy, as well as high stability characteristics [5,6]. Sliding-mode control (SMC)-based robust control techniques have been proven to be a successful method for controlling dynamic systems under uncertainties such as in the case of drones. SMC techniques have gained popularity because of their ability to handle both parameter fluctuations and disturbance rejection, which is particularly helpful in real-world applications. Finite-time stabilization control has been thoroughly investigated over the last few decades.

Cable-suspended aerial transportation systems, one of the most common types of aerial transportation systems, have been under intensive investigation by researchers. In this direction, the aim of the present paper is to design a fixed-time controller for both the altitude and yaw of a mini-drone and implement the design control law under different scenarios of suspended mass weights. A practical facility based on the Mambo multicopter developed by Parrot SA, as shown in Figure 1, was used for the practical experimental setup. To achieve this study's objectives, the differentially flat hybrid nature of the quadrotor aerial transportation system is first established. It should be noted that [7–12] address the modeling, controller design, and experimental validation of an unmanned aerial transportation system with flexible connectivity between the quadrotor and the payload. Researchers have unavoidably looked at robust control to run a quadrotor under uncertain conditions. However, adaptive control systems [7,8,12] require a priori knowledge of the system structure and bounds on external disturbances, whereas robust control approaches depend on accurate knowledge of the mass matrix. Due to unknown payloads and outside disturbances, it is often challenging to satisfy such limitations in real-world situations. Nevertheless, as most current research focuses on aerial transportation systems with fixed-length cables, raising and lowering the payload can only be accomplished by varying the height of the quadrotor. The demand for limited area crossing or offshore sample collecting cannot always be satisfied by fixed-length cable transportation. Specifically, while traversing a cave with a fixed-length cable, a quadrotor or payload may run into an obstruction.

Finite-time stability, as opposed to the more well-known asymptotic stability, ensures that the settling time is finite rather than infinite [13]. Additionally, finite-time stability achieves higher accuracy and better robustness [6]. Numerous methods, including homogeneity and terminal sliding mode, have been used to establish finite-time stability [13]. Fixed-time stabilization control has been recently developed. Its settling time is independent of the initial conditions of the system [14]. The main goal of this study is to design a fixed-time controller for yaw and altitude motion that is subject to disturbances. The primary novelties and contributions of this work can be summarized as follows when compared to the currently used methods:

- Utilizing sliding-mode control and the fixed-time stability concepts to design a fixed-time controller approach.
- Employing the suggested sliding mode to account for outside disturbances and modeling uncertainties without knowing in advance what their upper bounds are, and then using the specified sliding-mode controller to account for all of their combined effects.
- Choosing a suitable candidate Lyapunov function and establishing a settling time function (which is independent of the system's initial conditions) to help prove the closed-loop system's fixed-time stability.
- By considering modeling uncertainties for the stability analysis and evaluating resilience in a real application utilizing a mini-drone, the suggested method's robustness will be demonstrated.

Figure 1. Mambo multicopter: a small UAS developed by Parrot SA.

2. Problem Formulation

The dynamics of the quadrotor are considered as in [15,16]:

$$\begin{cases} \dot{p} = v \\ \dot{v} = \frac{1}{m}(Ł_{jb}(\delta)\Xi_T + \Xi_d(\chi,\dot{\chi},t)) - g \\ \dot{\delta} = Ł_T(\delta)\Omega \\ J(\delta)\dot{\Omega} = -\Omega \times J(\delta)\Omega + \mu + \mu_d(\chi,\dot{\chi},t) \end{cases} \tag{1}$$

where $\chi = \left[p^T\ v^T\ \delta^T\ \Omega^T\right]$, $p \in \mathbf{R}^3$ represents the position in the inertial frame, $v \in \mathbf{R}^3$ denotes the velocity, $\delta = [\phi\ \theta\ \psi]^T \in \mathbb{M} = (-\frac{\pi}{2}, \frac{\pi}{2})^2 \times (-\pi, \pi)$ represents the attitude of the quadrotor, and ϕ, θ, and ψ denote the roll, pitch, and yaw angles, respectively. $\Omega = \left[\Omega_\phi\ \Omega_\theta\ \Omega_\psi\right]^T$ denotes the angular velocity in the inertial frame; $\Xi_T = [0\ 0\ \Xi_z]^T$ denotes the controlled thrust; μ denotes the controlled torque in the inertial frame; $Ł_{jb} : \mathbb{M} \to SO(3)$ denotes the rotation matrix between the body-fixed frame and the inertial frame; $SO(3)$ denotes the special orthonormal group $SO(n) = \left\{Ł \in \mathbf{R}^{n\times n} : ŁŁ^T = I_n, \det Ł = 1\right\}$ in 3D; $I_n \in \mathbf{R}^{n\times n}$ denotes the identity matrix; $Ł_{jb}$ denotes the product of consecutive rotations around the x-, y-, and z-axes by angles ϕ, θ, and ψ, respectively; and $Ł_{jb}(\delta) = Ł_{z,\psi}(\psi)Ł_{y,\theta}(\theta)Ł_{x,\phi}(\phi)$, with $Ł_{z,\psi} : (-\pi, \pi) \to SO(3)$, $Ł_{y,\theta} : (-\frac{1}{2}\pi, \frac{1}{2}\pi) \to SO(3)$, and $Ł_{x,\phi} : (-\pi, \pi) \to SO(3)$ being the rotation matrices.

Moreover, $Ł_T :\to \mathbf{R}^{3\times 3}$ denotes the mapping of the angular speed to the Euler angles' time derivatives.

$$
Ł_T(\delta) = \begin{bmatrix} \dfrac{cos\psi}{cos\theta} & \dfrac{sin\psi}{cos\theta} & 0 \\ sin\psi & cos\psi & 0 \\ cos\psi.tang\theta & sin\psi.tang\theta & 1 \end{bmatrix}
$$

It is noted in this paper that $Ł_T$ is clearly stated for $\theta \in (-\frac{1}{2}\pi, \frac{1}{2}\pi)$. $\Xi_d(\chi, \dot{\chi}, t) = \left[\Xi_{d,x,y}^T \; \Xi_{d,z}\right]^T$ and $\mu_d = \mu_d(\chi, \dot{\chi}, t)$ are unmodeled aerodynamic forces and moments such as drag, hub forces, or ground and gyroscopic effects, as well as exogenous disturbances; χ and $\dot{\chi}$ represent two functions that exhibit continuity and are uniformly bounded in time; $g = [0\;0\;g]^T \in \mathbf{R}^3$ denotes the constant gravity vector; $m \in \mathbf{R}$ denotes the mass; and $J \in \mathbf{R}^3$ represents the moment inertia.

In this article, we look at the tracking control problem for given reference trajectories that change over time $p_r = \left[p_{x,r}\; p_{y,r}\; p_{z,r}\right]^T : [0, \infty) \to \mathbf{R}^3, \psi_r : [0, \infty) \to \mathbf{R}$ for the position and yaw angles under the specified conditions. We consider p_r and ψ_r to be time functions that are smooth and possess bounded first and second derivatives.

To achieve the benefits of minimum overshoot, convergence speed, and a minimum steady-state error as outlined in Section 2, the tracking error signal needs to remain within specific time-dependent functions, which form a funnel. It is important to note that the UAV model (1) is underactuated, but this can be resolved through the use of virtual control signals. To achieve the desired trajectory tracking performance for the position and yaw angle, we modify the virtual controls. In particular, the objective of the controls is to ensure that the errors converge to zero in a short time.

$$
\begin{aligned}
&\xi_p = \left[\xi_{px}\; \xi_{py}\; \xi_{pz}\right]^T = p - p_r \\
&\xi_\psi = \psi - \psi_r;\; \xi_\theta = \theta - \theta_r;\; \xi_\phi = \phi - \phi_r
\end{aligned} \tag{2}
$$

Remark 1. *The main advantages of the proposed technique are that it ensures fixed-time stability, accurate/fast tracking, and robustness against uncertainties. However, a major drawback of the technique is the chattering phenomenon.*

3. Robust Fixed-Time Sliding-Mode Controller

The main objective of this section is to design a fixed-time controller for the altitude/yaw tracking control in the presence of disturbances. Similar to [6], the quadrotor has six subsystems: three positions (x, y, z) and three orientations (ϕ, θ, ψ). In this paper, the horizontal position and the tilting angles (roll and pitch angles) are controlled by a simple PID. The fixed-time controller is implemented only for altitude and yaw movements. Let us define the position control signals as

$$
\begin{aligned}
\Lambda_x &= k_{px}\xi_{px} + k_{dx}\dot{\xi}_{px} + k_{px}\int \xi_{px} d\tau \\
\Lambda_y &= k_{py}\xi_{py} + k_{dy}\dot{\xi}_{py} + k_{py}\int \xi_{py} d\tau
\end{aligned} \tag{3}
$$

where k_{jx} and k_{jy} for $j = p, d, i$ are positive gains. Using the model system in (1) to define the virtual controls, the underactuated problem is solved [6].

$$
\Lambda = \begin{bmatrix} \Lambda_x \\ \Lambda_y \end{bmatrix} = \begin{bmatrix} (\cos\phi_r \sin\theta_r \cos\psi_r + \sin\phi_r \sin\psi(t))\frac{\Xi_z}{m} \\ (\cos\phi_r \sin\theta_r \sin\psi_r - \sin\phi_r \cos\psi_r)\frac{\Xi_z}{m} \end{bmatrix} \tag{4}
$$

Based on (4), the desired tilting angles can be designed as

$$
\phi_r = \arcsin(\Lambda_x \sin\psi_r - \Lambda_x \sin\psi_r) \tag{5a}
$$

$$
\theta_r = \arcsin(\frac{\cos\psi_r \Lambda_x + \sin\psi_r \Lambda_y}{\cos\phi_r}) \tag{5b}
$$

where ψ_r is the yaw reference and Λ is the virtual position-loop control vector designed in (3). The attitude-loop control input signals, including the rolling and pitching torques, are given by:

$$\begin{aligned}\Xi_\phi &= k_{p\phi}\xi_\phi + k_{d\phi}\dot{\xi}_\phi + k_{i\phi}\int \xi_\phi d\tau \\ \Xi_\theta &= k_{p\theta}\xi_\theta + k_{d\theta}\dot{\xi}_\theta + k_{i\theta}\int \xi_\theta d\tau\end{aligned} \tag{6}$$

where $k_{j\phi}$ and $k_{j\theta}$ for $j = p, d, i$ are positive gains. In the following part, a fixed-time control is presented for the altitude/yaw motion. The altitude/yaw dynamics can be formulated as a second-order non-linear system with uncertainties.

$$\begin{aligned}\dot{\mathcal{X}}_1 &= \mathcal{X}_2 \\ \dot{\mathcal{X}}_2 &= \varphi_1(\mathcal{X}) + \varphi_2(\mathcal{X})\Xi + d(t)\end{aligned} \tag{7}$$

$\mathcal{X}_i = \{p_z, \dot{p}_z, \psi, \dot{\psi}\}$ represents the state; Ξ are the control inputs; $\varphi_1(\mathcal{X})$ and $\varphi_2(\mathcal{X})$ are non-linear functions satisfying $\varphi_1(0) = 0$, $\varphi_2(\mathcal{X}) \neq 0$; and $d(t)$ represents disturbances with $|d(t)| < d_{sup}$. Consider the standard sliding variable as:

$$s_{pz} = k_{pz}\xi_{pz} + \dot{\xi}_{pz} + k_{iz}\int \xi_{pz} d\tau \tag{8a}$$

$$s_\psi = k_{p\psi}\xi_\psi + \dot{\xi}_\psi + k_{i\psi}\int \xi_\psi d\tau \tag{8b}$$

where k_{jz} and $k_{j\psi}$ for $j = p, d, i$ are positive gains. The proposed control is based on the integral sliding-mode surface and switching law. There are two controllers: the first is the equivalent law that is generated by setting $\{s_{pz}, s_\psi\} = 0$. Hence, the equivalent controllers are given by:

$$\Xi_{ze} = -\frac{1}{\varphi_{z2}}\{k_{pz}\dot{\xi}_{pz} + k_{iz}\xi_{pz} + \varphi_{z1}\} \tag{9a}$$

$$\Xi_{\psi e} = -\frac{1}{\varphi_{\psi 2}}\{k_{p\psi}\dot{\xi}_\psi + k_{i\psi}\xi_\psi + k_{\psi 1} + \varphi_{\psi 1}\} \tag{9b}$$

In order to achieve fixed-time stability, switching controllers are added to the equivalent controllers as follows:

$$\Xi_z = \Xi_{ze} + \Xi_{zs} \tag{10}$$

and

$$\Xi_\psi = \Xi_{\psi e} + \Xi_{\psi s} \tag{11}$$

where the switching control laws can be defined as:

$$\Xi_{zs} = -\frac{1}{\varphi_{z2}}\{k_{z1}sgn(s_{pz}) + k_{z4}s_{pz} + k_{z2}|s_{pz}|^{\alpha_{pz}}sgn(s_{pz}) + k_{z3}|s_{pz}|^{\gamma_{pz}}sgn(s_{pz})\} \tag{12a}$$

$$\Xi_{\psi s} = -\frac{1}{\varphi_{\psi 2}}\{k_{\psi 1}sgn(s_\psi) + k_{\psi 4}s_\psi + k_{\psi 2}|s_\psi|^{\alpha_\psi}sgn(s_\psi) + k_{\psi 3}|s_\psi|^{\gamma_\psi}sgn(s_\psi)\} \tag{12b}$$

where $\alpha_j > 1$, $\gamma_j < 1$, and $k_{\psi i}$, k_{zi} represent positive gains. The functions φ_{i1} and φ_{i2} are defined in (1).

Theorem 1. *The closed-loop systems* $\{(7),(8), (10)\}$ *reach the PID sliding surface* $\{s_i(0) = 0\}$ *in the following fixed time:*

$$T_{s0}(\mathcal{X}) \leq \frac{1}{(k_{j1} - d_{sup})} + \frac{1}{k_{j2}(\alpha_j - 1)} + \frac{1}{k_{j3}(1 - \gamma_j)} \tag{13}$$

We need the following Lemma to prove the above theorem.

Lemma 1. *Consider the system*

$$\dot{z} = \Psi(z), \quad z \in \mathbf{R} \quad and \quad z(0) = z_0 \tag{14}$$

If there is a positively definite, continuously differentiable, radially unbounded function $V(x) > 0$ such that:

$$\dot{V} \leq -\beta_1 V^a - \beta_2 V^b \tag{15}$$

where $x \in \mathbf{R}$, $\beta_i > 0$ and $b > 1, 0 < a < 1$, then the system (14) is globally FxT stable, and the estimation of the settling time satisfies

$$T(z_0) \leq \frac{1}{\beta_1(1-a)} + \frac{1}{\beta_2(b-1)} \tag{16}$$

Proof. Let us examine the time derivative of the sliding surface given by

$$\begin{aligned} \dot{s}_i =& k_{pz}\dot{\xi}_i + \varphi_1(\mathcal{X}) + \varphi_2(\mathcal{X})\Xi + d(t) + k_{iz}\xi_i \\ =& - k_{i1}sgn(s_i) - k_{i4}s_i - k_{i2}|s_i|^{\alpha_i}sgn(s_\psi) \\ & - k_{i3}|s_i|^{\gamma_i}sgn(s_i) + d(t) \end{aligned} \tag{17}$$

Consider the following Lyapunov function as $V = s_i^2$. Then, its derivative is given as

$$\begin{aligned} \dot{V} =& - 2s_i[k_{i1}sgn(s_i) - k_{i4}s_i - k_{i2}|s_i|^{\alpha_i}sgn(s_i) \\ & - k_{i3}|s_i|^{\gamma_i}sgn(s_i) + d(t)] \\ \leq& - 2k_{i1}|s_i| - 2k_{i2}|s_i|^{\alpha_i+1} - 2k_{i3}|s_i|^{\gamma_i+1} + 2d_{sup} \\ \dot{V} \leq& -2(k_{i1} - d_{sup})V^{0.5} - 2k_{i2}V^{\frac{\alpha_i+1}{2}} - 2k_{i3}V^{\frac{\gamma_i+1}{2}} \end{aligned} \tag{18}$$

In Lemma 1, we have

$$T_{s0}(\mathcal{X})) \leq \frac{1}{(k_{j1} - d_{sup})} + \frac{1}{k_{j2}(\alpha_j - 1)} + \frac{1}{k_{j3}(1 - \gamma_j)} \tag{19}$$

From the results given in (18) and (19), we can conclude the proof of fixed-time stability. □

4. Experimental Validation

This section presents experimental results to validate the effectiveness of the proposed fixed-time control scheme for the position and attitude tracking of quadrotors. The laboratory experimental test bench is displayed in Figure 2. The test bench comprised an inertial measurement unit with six DOF (three-axis accelerometer and three-axis gyroscope), an ultrasonic sensor, and pressure sensors to determine the quadrotor's altitude; a 120 × 160-pixel camera capable of capturing pictures at 60 frames per second; an IMU inertial navigation system used to measure the horizontal displacement; and a Kalman filtering system for the captured images. The proposed control system was built in a Matlab/Simulink environment, which was connected to the Parrot Mambo via Bluetooth 4.0. The Matlab model was then converted to C code, which was uploaded and tested on a Parrot Mambo mini-drone in real time.

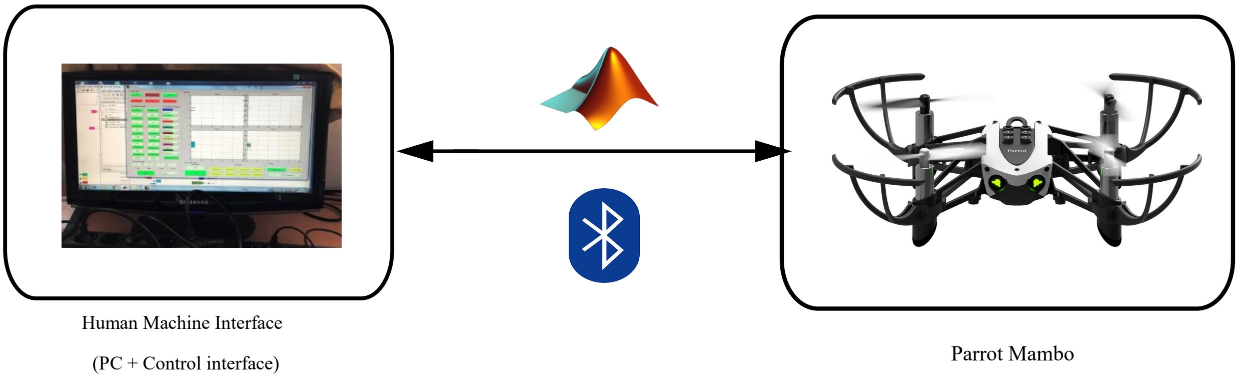

Figure 2. Configuration of the experimental test setup.

To check the robustness of our fixed-time controller, three scenarios in terms of load changes were considered, as shown in Figure 3. In the first scenario, the drone was commanded to track the desired altitude and yaw motion while carrying an additional load of 10 g on the nominal mass. The second scenario involved controlling the drone with an added load of 20 g on the nominal mass. In the third scenario, the mass of the drone was increased by 30 g to evaluate the performance of the proposed method. The experimental parameters for all three scenarios are presented in Table 1. It is important to note that these scenarios are common in last-mile delivery applications in outdoor logistics, where the drone, which already has a limited payload capacity, is expected to transport the maximum possible mass without being altered or sacrificing its main characteristics, particularly in terms of stability and robust trajectory tracking.

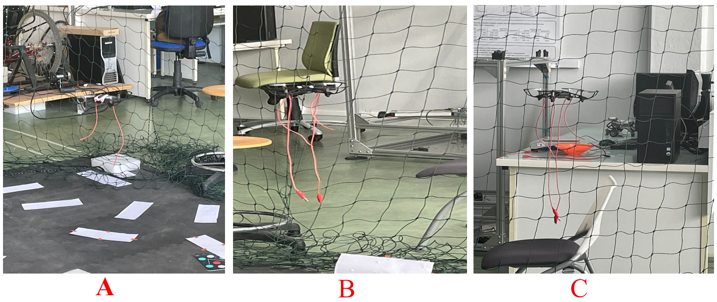

Figure 3. Three different scenarios for the quadrotor during the experiments with the proposed controller: (**A**) scenario with an added load of 10 g on the nominal mass, (**B**) scenario with an added load of 20 g on the nominal mass, and (**C**) scenario with an added load of 30 g on the nominal mass.

Table 1. Parameters in experiments.

Param.	Value	Param.	Value
m	69 g	J	10^{-5} diag [5.8 7.2 10] kgm^2
g	9.81 m/s^2	K_p	10^{-1} diag [6.2 4.5 6.9]
T_s	0.005 s	K_z	10^{-1} diag [1 1 1.5]
		K_R	10^{-2} diag [1.5 1.5 0.2]
		K_Ω	10^{-3} diag [2.2 2.2 0.7]

4.1. Scenario 1

Figures 4–7 show the tracking performance in the first scenario. As shown in Figure 4, all state variables converged to their references in the short term. For example, from the motion along the z-axis, it can be seen that the proposed method was capable of tracking the desired altitude with 10 g of mass disturbances. The tracking errors, including ξ_ϕ and ξ_{pz}, converged to zero, as shown in Figure 6. Furthermore, the control inputs shown in Figure 7 demonstrate that the control inputs Ξ_ϕ, Ξ_θ, and Ξ_ψ converged to zero, whereas the control input Ξ_z tracked the desired value with a smooth form to reduce the chattering phenomenon.

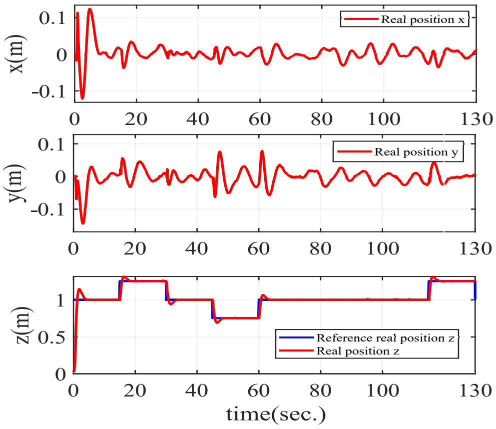

Figure 4. Experimental results of the position with a 10 g added load on the nominal mass.

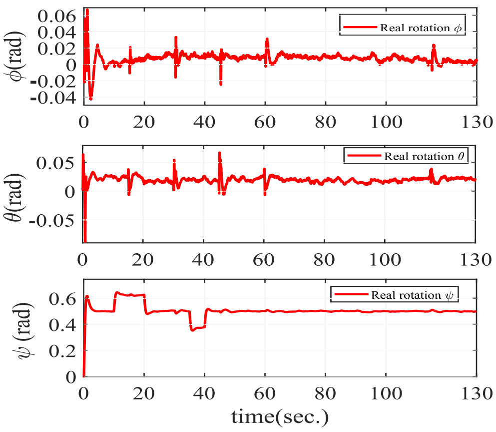

Figure 5. Experimental results of the attitude with a 10 g added load on the nominal mass.

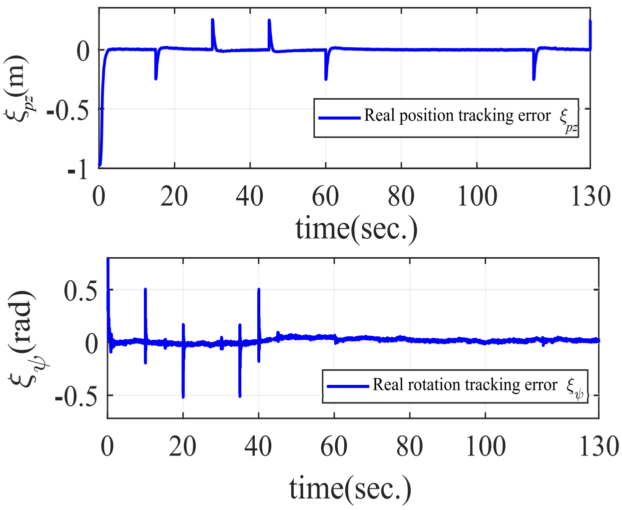

Figure 6. Experimental results of the tracking errors of the quadrotor with a 10 g added load on the nominal mass.

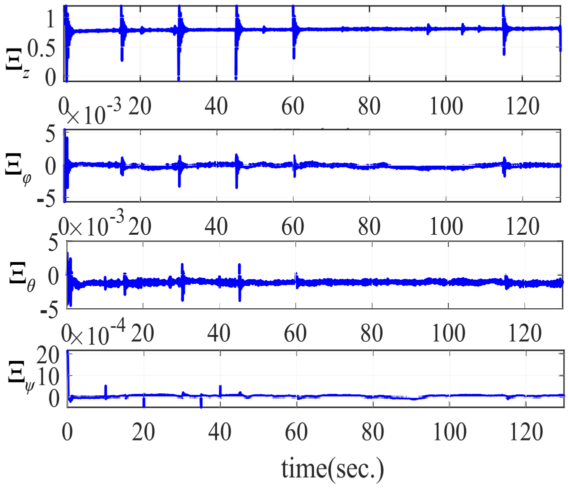

Figure 7. Experimental results of the control inputs of the quadrotor with a 10 g added load on the nominal mass.

4.2. Scenario 2

In the second scenario, the proposed method was evaluated under a 20 g mass disturbance, as shown in Figures 8–15. The real position (x, y, z) and real attitude (ϕ, θ, ψ) closely followed their reference values, despite the presence of an increased disturbance mass of 20 g, as presented in Figures 8 and 9. The tracking errors converged quickly to zero, as shown in Figure 10. The amplitudes of the inputs shown in Figure 11 converged to their desired values with reduced chattering.

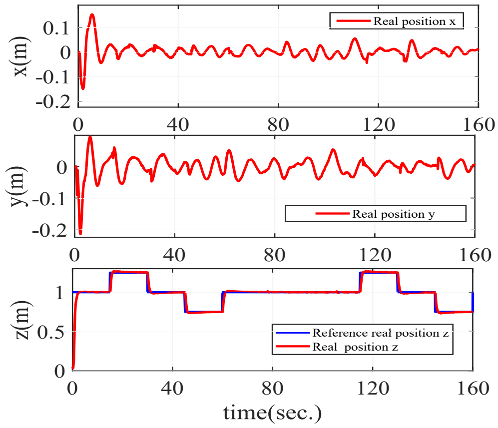

Figure 8. Experimental results of the position with a 10 g added load on the nominal mass.

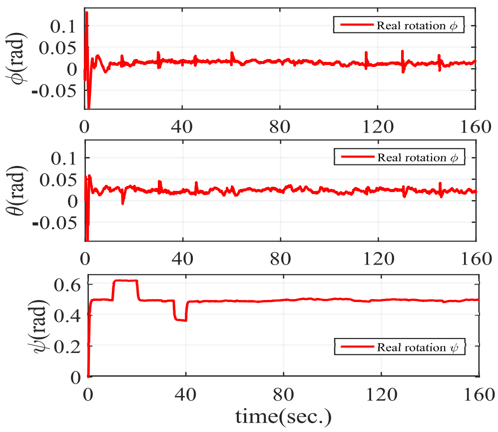

Figure 9. Experimental results of the attitude with a 10 g added load on the nominal mass.

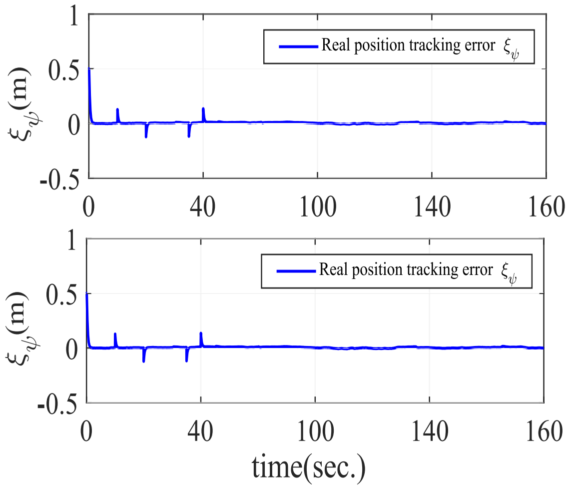

Figure 10. Experimental results of the tracking errors of the quadrotor with a 10 g added load on the nominal mass.

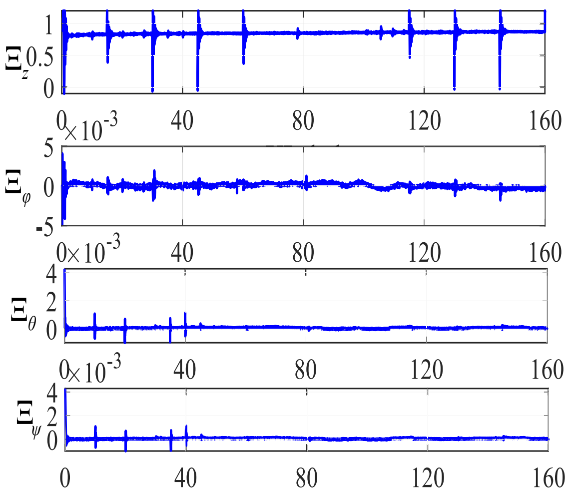

Figure 11. Experimental results of control inputs of the quadrotor with a 10 g added load on the nominal mass.

4.3. Scenario 3

In the third scenario, a disturbance mass of 30 g was added to the nominal mass of the quadrotor to further demonstrate the robustness of the proposed method. Figures 12–15 show the responses with a 30 g load mass. The state variables closely tracked their reference values in response to the proposed method. In addition, the motion along the z-axis and the yaw ψ exhibited faster convergence and less chattering using the proposed Fxt control. By employing the proposed method, it is possible to achieve small position errors on the z-axis and yaw ψ errors, as shown in Figure 14. Despite the imperfect tracking of the commanded inputs by the drone, the proposed method effectively reduces these errors. We can see in Figure 15 that the control inputs Ξ_ϕ, Ξ_θ, and Ξ_ψ converged to zero, whereas Ξ_z tracked the desired value, despite the presence of a significant disturbance in the mass. In addition, the control inputs were smooth with lower gains (upper bound of the inputs), demonstrating that the drone was more stable with these inputs.

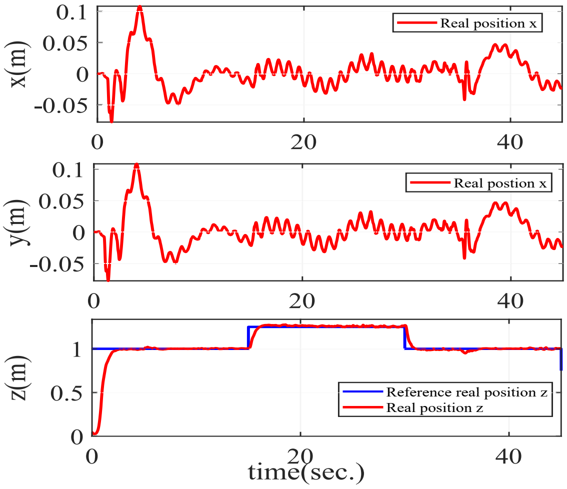

Figure 12. Experimental results of the position with a 10 g added load on the nominal mass.

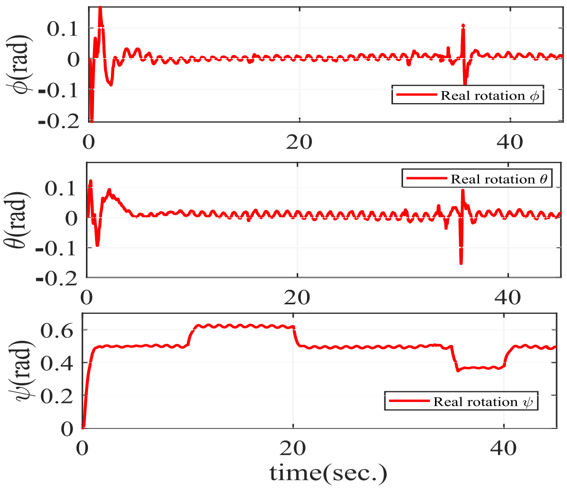

Figure 13. Experimental results of the attitude with a 10 g added load on the nominal mass.

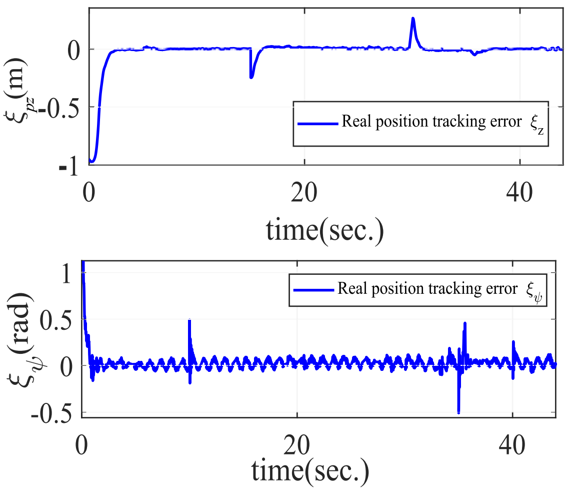

Figure 14. Experimental results of the tracking errors of the quadrotor with a 10 g added load on the nominal mass.

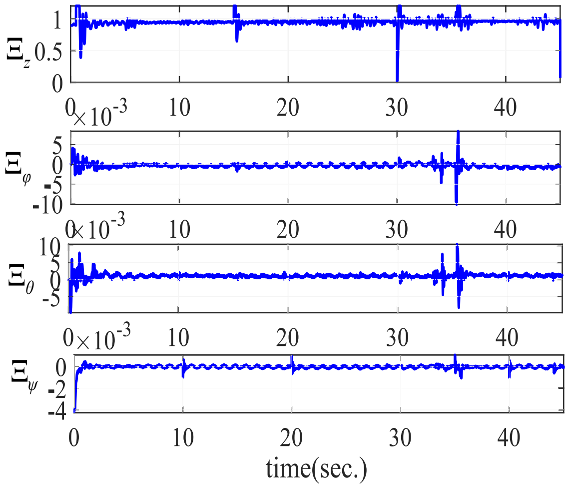

Figure 15. Experimental results of control inputs of the quadrotor with a 10 g added load on the nominal mass.

5. Conclusions

In this paper, a fixed-time control strategy has been designed to achieve fixed-time stability of the altitude/yaw motion of a mini-drone subjected to uncertainties. Moreover, for the horizontal position and tilting angle subsystems, a simple PID has been used. The stability of the FxT approach has been proven using the Lyapunov theory. By adjusting the parameters of the FxT controller, satisfactory performance was achieved in the predefined tracking of the altitude/yaw motion. The performance has been proven by experiment validation using a real drone. In the three scenarios presented above, the proposed FxT approach demonstrated excellent performance. Future research efforts will be directed at applying the proposed control strategy to multi-agent systems.

Author Contributions: M.L. and S.B.; methodology, M.L.; software, M.L.; validation, M.L., C.C., S.B. and S.K.; formal analysis, M.L. and C.C.; investigation, M.L.; resources, M.L. and C.C.; data curation, M.L.; writing—original draft preparation, M.L., C.C., S.B. and S.K.; writing—review and editing, M.L., C.C., S.B. and S.K.; visualization, M.L., C.C., S.B. and S.K.; supervision, M.L., S.B. and S.K.; project administration, S.B. and S.K.; funding acquisition, M.L., C.C., S.B. and S.K. All authors have read and agreed to the published version of the manuscript.

Funding: This research was funded by the Deputyship for Research & Innovation, Ministry of Education in Saudi Arabia funded this research work through the project number MoE-IF-UJ-22-04220772-2.

Data Availability Statement: Where no new data were created.

Acknowledgments: The authors extend their appreciation to the Deputyship for Research & Innovation, Ministry of Education in Saudi Arabia for funding this research work through the project number MoE-IF-UJ-22-04220772-2.

Conflicts of Interest: The authors declare no conflict of interest.

References

1. Wang, J.; Alattas, K.A.; Bouteraa, Y.; Mofid, O.; Mobayen, S. Adaptive finite-time backstepping control tracker for quadrotor UAV with model uncertainty and external disturbance. *Aerosp. Sci. Technol.* **2023**, *133*, 108088. [CrossRef]
2. Mofid, O.; Mobayen, S.; Zhang, C.; Esakki, B. Desired tracking of delayed quadrotor UAV under model uncertainty and wind disturbance using adaptive super-twisting terminal sliding mode control. *ISA Trans.* **2022**, *123*, 455–471. [CrossRef] [PubMed]
3. Nguyen, H.P.D.; Nguyen, D.D. Drone Application in Smart Cities: The General Overview of Security Vulnerabilities and Countermeasures for Data Communication. In *Development and Future of Internet of Drones (IoD): Insights, Trends and Road Ahead*; Krishnamurthi, R., Nayyar, A., Hassanien, A.E., Eds.; Studies in Systems, Decision and Control; Springer International Publishing: Cham, Switzerland, 2021; pp. 185–210.
4. Yaacoub, J.-P.; Noura, H.; Salman, O.; Chehab, A. Security analysis of drones systems: Attacks, limitations, and recommendations. *Internet Things* **2020**, *11*, 100218. [CrossRef]

5. Utkin, V. Variable structure systems with sliding modes. *Int. J. Robust Nonlinear Control* **1977**, *22*, 212–222. [CrossRef]
6. Labbadi, M.; Defoort, M.; Incremona, G.P.; Djemai, M. Fractional-order integral terminal sliding-mode control for perturbed nonlinear systems with application to quadrotors. *Int. J. Robust Nonlinear Control* **2023**. [CrossRef]
7. Sankaranarayanan, V.N.; Roy, S.; Baldi, S. Aerial transportation of unknown payloads: Adaptive path tracking for quadrotors. *IEEE Int. Conf. Intell. Robot. Syst.* **2020**, 7710–7715. [CrossRef]
8. Yang, S.; Xian, B. Energy-Based Nonlinear Adaptive Control Design for the Quadrotor UAV System with a Suspended Payload. *IEEE Trans. Ind. Electron.* **2020**, *67*, 2054–2064. [CrossRef]
9. Yang, S.; Xian, B. Exponential Regulation Control of a Quadrotor Unmanned Aerial Vehicle with a Suspended Payload. *IEEE Trans. Control Syst. Technol.* **2020**, *28*, 2762–2769. [CrossRef]
10. Liang, X.; Yu, H.; Zhang, Z.; Liu, H.; Fang, Y.; Han, J. Flexible Connection between the Quadrotor and the Payload: Modeling, Controller Design, and Experimental Validation. *IEEE Trans. Ind. Electron.* **2023**, *70*, 1870–1882. [CrossRef]
11. Guerrero-Sánchez, M.E.; Mercado-Ravell, D.A.; Lozano, R.; García-Beltrán, C.D. Swing-attenuation for a quadrotor transporting a cable-suspended payload. *ISA Trans.* **2017**, *68*, 433–449. [CrossRef] [PubMed]
12. Yu, H.; Liang, X.; Han, J.; Fang, Y. Adaptive Trajectory Tracking Control for the Quadrotor Aerial Transportation System Landing a Payload Onto the Mobile Platform. *IEEE Trans. Ind. Inform.* **2023**, 1–12. [CrossRef]
13. Bhat, S.P.; Bernstein, D.S. Finite-time stability of homogeneous systems. In Proceedings of the 1997 American Control Conference, Albuquerque, NM, USA, 6 June 1997; Volume 4, pp. 1073–1078.
14. Aouiti, C.; Hui, Q.; Jallouli, H.; Moulay, E. Sliding mode control-based fixed-time stabilization and synchronization of inertial neural networks with time-varying delays. *Neural Comput. Appl.* **2021**, *33*, 11555–11572. [CrossRef]
15. Wu, Z.; Cheng, S.; Ackerman, K.A.; Gahlawat, A.; Lakshmanan, A.; Zhao, P.; Hovakimyan, N. Adaptive Augmentation for Geometric Tracking Control of Quadrotors. In Proceedings of the 2022 International Conference on Robotics and Automation (ICRA), Philadelphia, PA, USA, 23–27 May 2022; pp. 1329–1336.
16. Vong, C.H.; Ryan, K.; Chung, H. Integral Backstepping Position Control for Quadrotors in Tunnel-Like Confined Environments. In Proceedings of the 2019 International Conference on Robotics and Automation (ICRA), Montreal, QC, Canada, 20–24 May 2019; pp. 6425–6431.